J. Fluid Mech. (1997), *vol.* 336, *pp.* 221–244

On the motion of gas bubbles in homogeneous isotropic turbulence

By P. D. M. SPELT AND A. BIESHEUVEL

J. M. Burgers Centre for Fluid Mechanics, University of Twente,
PO Box 217, 7500 AE Enschede, The Netherlands

(Received 2 October 1995 and in revised form 6 November 1996)

This paper is concerned with the motion of small gas bubbles, equivalent diameter about 1.0 mm, in isotropic turbulent flows. Data on the mean velocity of rise and the dispersion of the bubbles have been obtained numerically by simulating the turbulence as a sum of Fourier modes with random phases and amplitudes determined by the Kraichnan and the von Kármán–Pao energy-spectrum functions, and by calculating the bubble trajectories from a reasonably well-established equation of motion. The data cover the range $\beta \leqslant 1$, where β is the ratio between the turbulence intensity and the velocity of rise of the bubbles in still fluid. An approximate analysis based on the assumption that β is small yields results that compare favourably with the numerical data, and clarifies the important role played by the lift forces exerted by the fluid.

1. Introduction

Generally, the motion of a gas bubble moving with velocity $\boldsymbol{V}(t)$ through a turbulent fluid, characterized by a velocity field $\boldsymbol{U}(\boldsymbol{x}, t)$, is governed by the stochastic equation

$$\frac{\mathrm{d}\boldsymbol{V}}{\mathrm{d}t} = \mathscr{F}(\boldsymbol{V}(t), \boldsymbol{U}(\boldsymbol{X}(t), t)),$$

where $\boldsymbol{X}(t)$ denotes the position of the bubble, and $\mathscr{F}$ is a (nonlinear) functional of the fluid and bubble velocities. To obtain statistical properties of the bubble motion one has to solve this equation, supposing that it is known, and express these statistical properties in terms of those of the turbulence along the (unknown) path of the bubble. Information on the characteristics of the turbulence is usually only available from measurements at fixed positions, so one is faced with the problem of relating Eulerian characteristics to Lagrangian characteristics. It will be clear that analytical solutions can only be found in rare cases, which allow special assumptions to be made, and that numerical simulations offer a better chance to gain some understanding of the motion of bubbles in turbulent flows. In this paper we present results of approximate analyses and numerical simulations of the motion of gas bubbles rising at high Reynolds numbers through homogeneous isotropic turbulence.

The turbulent velocity field is simulated by a large number of Fourier modes varying randomly in space and time, chosen in such a way that the associated energy-spectrum function has the desired form. This technique was proposed by Kraichnan (1970) to simulate turbulent self-diffusion, and modified versions have been widely used to study the settling and dispersion of small rigid particles in isotropic turbulence (e.g. Maxey 1987*a*; Fung 1993; Mei 1994; Wang & Stock 1994). The energy-spectrum

functions chosen in this paper are that used originally by Kraichnan (1970) and the von Kármán–Pao spectrum (e.g. Helland, Van Atta & Stegen 1977); in both cases the frequency dependence is chosen in accordance with the results of numerical simulations by Hunt, Buell & Wray (1987). Details on the method of simulation are given in §2.

The bubble motion is taken to be governed by an equation proposed by Thomas *et al.* (1984) and used by these authors to study the interaction of gas bubbles with coherent vortices in a plunging water jet (see also Sene, Hunt & Thomas 1994). The forces exerted on a bubble by the surrounding fluid are described by a superposition of the force on a rigid sphere in an inviscid unsteady non-uniform rotational flow (Auton, Hunt & Prud'homme 1988), and the drag experienced by a spherical gas bubble rising steadily at high Reynolds number in still fluid. A good approximation for this drag force can be obtained by a calculation based on viscous potential flow theory (Moore 1963). The equation of motion of the bubbles and its underlying assumptions, together with the numerical methods used to calculate the bubble trajectories and the associated statistics, are described in §3.

Numerical and approximate analytical results for the motion of the bubbles are discussed in §§4 and 5. Section 4 is concerned with the effects of the turbulence on the mean velocity of rise of the bubbles, and §5 considers their velocity fluctuations and dispersion. In the analyses, which use ideas from Maxey (1987*a*), it is assumed that β, the ratio between the turbulence intensity and the velocity of rise of the bubble in quiescent fluid, is small. The numerical simulations cover the range $\beta \leqslant 1$. It is found that the velocity of rise is markedly reduced, down to 50% of the value in still fluid. The longitudinal and lateral dispersion processes over large times can be associated with diffusion coefficients. These coefficients have a value which is less than 40% of that for fluid particles when the integral length scale of the turbulence is five times the length scale that characterizes the velocity relaxation of the bubbles; however, when these length scales are approximately equal, the diffusion coefficients for the bubbles become considerably larger than those for fluid particles for values of β larger than 0.5. A simple explanation for this is proposed at the end of the paper.

2. Simulation of the turbulent velocity field

The velocity field is represented as a Fourier series

$$\boldsymbol{u}(\boldsymbol{x},t) = \sum_{n=1}^{N} \left[\tilde{\boldsymbol{a}}^{(n)} \cos(\boldsymbol{k}^{(n)} \cdot \boldsymbol{x} + \omega^{(n)} t) + \tilde{\boldsymbol{b}}^{(n)} \sin(\boldsymbol{k}^{(n)} \cdot \boldsymbol{x} + \omega^{(n)} t) \right], \tag{2.1}$$

with random coefficients $\tilde{a}_i^{(n)}$, $\tilde{b}_i^{(n)}$ $(i = 1, 2, 3)$, and random wave vector components $k_i^{(n)}$ and frequencies $\omega^{(n)}$. The number of modes N is large, typically 200 in our simulations. By taking

$$\tilde{\boldsymbol{a}}^{(n)} = \boldsymbol{a}^{(n)} \times \frac{\boldsymbol{k}^{(n)}}{|\boldsymbol{k}^{(n)}|}, \quad \tilde{\boldsymbol{b}}^{(n)} = \boldsymbol{b}^{(n)} \times \frac{\boldsymbol{k}^{(n)}}{|\boldsymbol{k}^{(n)}|},$$

it is assured that the velocity field is solenoidal.

The coefficients $\boldsymbol{a}^{(n)}$ and $\boldsymbol{b}^{(n)}$ are chosen such that the velocity field is isotropic, with a given turbulent intensity, and the discretization of wavenumber space is such that,

for a given energy-spectrum function $E(k)$, there is equal energy

$$\int_{k^{(n-1)}}^{k^{(n)}} E(k)\mathrm{d}k$$

associated with each wave vector $\boldsymbol{k}^{(n)}$. For isotropic turbulence

$$\tfrac{3}{2}\sum_{n}^{N}\overline{|\boldsymbol{u}^{(n)}|^2} = \tfrac{1}{3}\sum_{n}^{N}\overline{|\boldsymbol{a}^{(n)}|^2} = \tfrac{1}{3}\sum_{n}^{N}\overline{|\boldsymbol{b}^{(n)}|^2} = \tfrac{3}{2}u_0^2,$$

where the overline denotes ensemble averaging, and

$$\tfrac{3}{2}u_0^2 = \int_0^\infty E(k)\mathrm{d}k. \tag{2.2}$$

Accordingly, to obtain the wave vectors $\boldsymbol{k}^{(n)}$, the direction of this vector is chosen randomly uniform and the length is determined by the prescription

$$\int_0^{k^{(n)}} E(k)\mathrm{d}k = \tfrac{3}{2}\left(n-\tfrac{1}{2}\right)u_0^2/N.$$

Next, the random coefficients $\boldsymbol{a}^{(n)}$ and $\boldsymbol{b}^{(n)}$ are determined by again choosing a uniformly random direction and choosing a length from a Gaussian distribution with zero mean, and variance $\frac{9}{2}u_0^2/N$.

The simulations have been performed with two forms of the energy-spectrum function: the Kraichnan spectrum function, which is representative for low-Reynolds-number turbulence behind a grid (Batchelor & Townsend 1948), and the von Kármán–Pao spectrum function, which was found by Helland *et al.* (1977) to well represent data for high-Reynolds-number turbulence. The Kraichnan spectrum function is given by

$$E(k) = \frac{16}{\left(\frac{1}{2}\pi\right)^{1/2}}\frac{u_0^2k^4}{k_0^5}\exp\left(-2k^2/k_0^2\right),$$

which has a maximum at the wavelength k_0. The simulated velocity field is thus specified by the choice of the velocity scale u_0 and the lengthscale $1/k_0$; this automatically fixes other turbulence scales like the longitudinal integral scale L_{11}, defined as

$$L_{11} = \frac{\pi}{2u_0^2}\int_0^\infty \frac{E(k)}{k}\,\mathrm{d}k, \tag{2.3}$$

and the Taylor microscale λ,

$$\frac{1}{\lambda^2} = \frac{2}{15u_0^2}\int_0^\infty k^2E(k)\,\mathrm{d}k, \tag{2.4}$$

since for the Kraichnan spectrum it can be shown from (2.3) and (2.4) that

$$L_{11} = \frac{(2\pi)^{1/2}}{k_0}, \quad \lambda = \frac{2}{k_0}.$$

A convenient way of writing the von Kármán–Pao spectrum function is

$$E(k) = \alpha_K\frac{v^2}{\eta}\left(\frac{L}{\eta}\right)^{5/3}\frac{(kL)^4}{[1+(kL)^2]^{17/6}}\exp\left(-\tfrac{3}{2}\beta_K(k\eta)^{4/3}\right),$$

which contains, for a given value of the viscosity v, four parameters: α_K, β_K, an

integral length scale L, and the Kolmogorov length scale η. The spectrum is again made fully determinate by a specification of the turbulent intensity u_0 and one of the length scales L_{11} or λ. This is achieved by using relation (2.2), one of (2.3) and (2.4), the fact that for isotropic turbulence the rate of energy dissipation ϵ can be expressed as

$$\epsilon = 15\nu\frac{u_0^2}{\lambda^2} = \frac{\nu^3}{\eta^4}, \tag{2.5}$$

and the empirical relationship (Sreenivasan 1984)

$$\frac{\eta}{L_{11}} \simeq 1.0\left(\frac{u_0 L_{11}}{\nu}\right)^{-3/4}. \tag{2.6}$$

For our simulations we took as the viscosity of the fluid that of water at a temperature of 20°C, and, to allow for comparisons, the velocity scale u_0 and either the longitudinal integral scale L_{11} or the Taylor microscale λ were taken equal to that used in the simulations with the Kraichnan energy-spectrum function.

Figure 1 illustrates that by taking the two longitudinal integral scales equal, for a fixed value of u_0, the available energy in the Kraichnan spectrum is partly shifted towards the higher wavenumbers. Since $(1/\lambda)^2$ is a measure of the dispersion of energy in wavenumber space, this means that the Taylor microscale becomes smaller. By taking equal Taylor microscales the shift towards higher wavenumbers is less substantial and a considerable amount of energy is also converted to low wavenumbers. Thus, the integral scales become larger and, since these are a measure of the extent over which velocities are reasonably correlated, the typical size of eddies is increased. Combining the relations (2.5) and (2.6) gives

$$\frac{L_{11}}{\lambda^2} = \frac{u_0}{15\nu}, \tag{2.7}$$

which shows that, for a fixed value of the Taylor microscale, the longitudinal integral scale becomes larger in proportion with an increase in the turbulent intensity u_0, while for a fixed value of the longitudinal integral scale, the Taylor microscale shortens in proportion to $u_0^{1/2}$.

Finally, the frequencies $\omega^{(n)}$ are chosen randomly from a Gaussian distribution with zero mean, and standard deviation

$$\left(\overline{[\omega^{(n)}]^2}\right)^{1/2} = a^* u_0 k^{(n)}.$$

This implies that the energy spectrum $\mathscr{E}(k,\omega)$ has the form

$$\mathscr{E}(k,\omega) = E(k)\exp\left[-\frac{\omega^2}{2(a^* k u_0)^2}\right] / \left((2\pi)^{1/2}(a^* k u_0)\right). \tag{2.8}$$

The choice is motivated by the direct numerical simulations of Hunt *et al.* (1987), which show that a good approximation for $\mathscr{E}(k,\omega)$ is (2.8) with $a^* \simeq 0.40$ for $kL_{11} \leqslant 10$, and $a^* \simeq 0.51$ for $kL_{11} \geqslant 15$. We have performed simulations both with $a^* = 0.51$ and with $a^* = 0.40$ for the whole range of wave modes (and for all values of $R_\lambda = u_0\lambda/\nu$), but the results for the bubble motion appeared not to differ qualitatively.

2.1. *Structure of the turbulent velocity field*

To investigate whether the bubbles preferently sample certain regions of the turbulent velocity field we have used the flow structure classification of Hunt, Wray & Moin (1988; see also Wray & Hunt 1990). This classification distinguishes regions of the

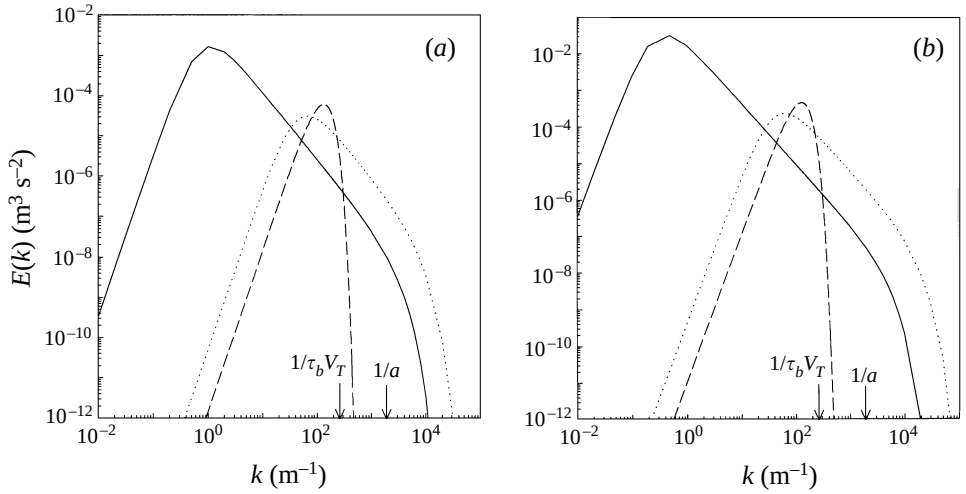

FIGURE 1. Examples of the energy-spectrum functions used in the numerical simulations, for (*a*) $\beta = 0.25$ and (*b*) $\beta = 0.66$, with β the ratio between the turbulence intensity and the bubble rise velocity in still fluid. - - -, Kraichnan spectrum; —, von Kármán–Pao spectrum with the same energy and Taylor microscale as the Kraichnan spectrum; ···, von Kármán–Pao spectrum with the same energy and integral length scale as the Kraichan spectrum. The arrows indicate the wavenumbers related to the relaxation length $\tau_b V_T$ and the radius a of the bubbles used in the simulations. The Taylor microscale and the integral length scale of the Kraichnan spectrum are 4 and 5 times the bubble relaxation length, respectively.

flow by a comparison of the second invariant of the rate-of-deformation tensor, defined as

$$\Pi = \frac{\partial u_i}{\partial x_j}\frac{\partial u_j}{\partial x_i} = e_{ij}^2 - \tfrac{1}{2}\omega_k^2,$$

with e_{ij} the rate-of-strain tensor and ω_k the vorticity, the pressure p and the magnitude of the velocity $|\boldsymbol{u}|$ with suitable threshold values. These could for instance be chosen as the root-mean-square values for the flow. Special zones in this classification are:
eddy zones: $\Pi < -\frac{1}{2}\Pi_{rms}$ and $p < -\frac{1}{2}p_{rms}$;
shear zones: $\Pi < -\frac{1}{2}\Pi_{rms}$ and $-\frac{1}{2}p_{rms} < p < p_{rms}$;
streaming zones: $|\Pi| < \frac{1}{2}\Pi_{rms}$ and $|\boldsymbol{u}| > u_0$;
convergence zones $\Pi > \Pi_{rms}$ and $p > p_{rms}$.

An expression for the second invariant in terms of the random coefficients $\boldsymbol{a}^{(n)}$, $\boldsymbol{b}^{(n)}$, the random wavenumber vectors $\boldsymbol{k}^{(n)}$ and frequencies $\omega^{(n)}$ follows readily by differentiating the series (2.1). To obtain an expression for the pressure in terms of these coefficients one may solve the Poisson equation

$$\nabla^2 p/\rho = -\Pi,$$

which yields

$$\frac{p(\boldsymbol{x},t)}{\rho} = \sum_{m\neq n=1}^{N}\sum_{n=1}^{N}\left[\alpha_{11}\,\cos\left(\boldsymbol{k}^{(+)}\cdot\boldsymbol{x}+\omega^{(+)}t\right)+\alpha_{12}\,\sin\left(\boldsymbol{k}^{(+)}\cdot\boldsymbol{x}+\omega^{(+)}t\right)\right]$$

$$+\sum_{m\neq n=1}^{N}\sum_{n=1}^{N}\left[\alpha_{21}\,\cos\left(\boldsymbol{k}^{(-)}\cdot\boldsymbol{x}+\omega^{(-)}t\right)+\alpha_{22}\,\sin\left(\boldsymbol{k}^{(-)}\cdot\boldsymbol{x}+\omega^{(-)}t\right)\right],$$

Zone	SB (KS)	WH (DNS)
eddy	16%	13%
shear	7%	6%
streaming	36%	25%
convergence	7%	4%

TABLE 1. Comparison of present results (SB) with those of Wray & Hunt (1990) (WH) for the average volume fraction drawn in to each zone

with

$$\boldsymbol{k}^{(+)} = \boldsymbol{k}^{(m)} + \boldsymbol{k}^{(n)}, \qquad \boldsymbol{k}^{(-)} = \boldsymbol{k}^{(m)} - \boldsymbol{k}^{(n)},$$
$$\omega^{(+)} = \omega^{(m)} + \omega^{(n)}, \qquad \omega^{(-)} = \omega^{(m)} - \omega^{(n)},$$

and

$$\alpha_{11} = -\frac{1}{2}\frac{(\tilde{\boldsymbol{a}}^{(m)} \cdot \boldsymbol{k}^{(+)})(\tilde{\boldsymbol{a}}^{(n)} \cdot \boldsymbol{k}^{(+)}) - (\tilde{\boldsymbol{b}}^{(m)} \cdot \boldsymbol{k}^{(+)})(\tilde{\boldsymbol{b}}^{(n)} \cdot \boldsymbol{k}^{(+)})}{|\boldsymbol{k}^{(+)}|^2},$$

$$\alpha_{12} = -\frac{1}{2}\frac{(\tilde{\boldsymbol{b}}^{(m)} \cdot \boldsymbol{k}^{(+)})(\tilde{\boldsymbol{a}}^{(n)} \cdot \boldsymbol{k}^{(+)}) + (\tilde{\boldsymbol{a}}^{(m)} \cdot \boldsymbol{k}^{(+)})(\tilde{\boldsymbol{b}}^{(n)} \cdot \boldsymbol{k}^{(+)})}{|\boldsymbol{k}^{(+)}|^2},$$

$$\alpha_{21} = -\frac{1}{2}\frac{(\tilde{\boldsymbol{a}}^{(m)} \cdot \boldsymbol{k}^{(-)})(\tilde{\boldsymbol{a}}^{(n)} \cdot \boldsymbol{k}^{(-)}) + (\tilde{\boldsymbol{b}}^{(m)} \cdot \boldsymbol{k}^{(-)})(\tilde{\boldsymbol{b}}^{(n)} \cdot \boldsymbol{k}^{(-)})}{|\boldsymbol{k}^{(-)}|^2},$$

$$\alpha_{22} = \frac{1}{2}\frac{(\tilde{\boldsymbol{b}}^{(m)} \cdot \boldsymbol{k}^{(-)})(\tilde{\boldsymbol{a}}^{(n)} \cdot \boldsymbol{k}^{(-)}) - (\tilde{\boldsymbol{a}}^{(m)} \cdot \boldsymbol{k}^{(-)})(\tilde{\boldsymbol{b}}^{(n)} \cdot \boldsymbol{k}^{(-)})}{|\boldsymbol{k}^{(-)}|^2}.$$

As an example the four zones are indicated in figure 2, which is a two-dimensional snapshot, dimensions $5L_{11}$, of a three-dimensional velocity field generated using the Kraichnan spectrum function. The flow in the eddy zones is clearly seen to swirl, while it diverges or converges in the convergence zones; the eddy zones appear to be surrounded by streaming zones. The general picture given by Wray & Hunt (1990), in a study using DNS with $R_\lambda \approx 25$, is that eddies, sometimes flanked by shear zones, pump fluid along streams, which may collide to form convergence zones, deflecting the streams away back toward the eddies.

The average volume fraction that is taken in by the zones was found not to depend much on the values of u_0 and k_0. Table 1 gives a comparison of our results with those of Wray & Hunt (1990); they agree fairly well.

2.2. *Discussion*

An extensive comparison of the properties of the flow fields generated by our method of kinematic simulation, with those found by other methods and with well-known analytical results, is given in Spelt (1996). As is commonly found with this method of simulation, the two-point Eulerian statistics are represented well, but it fails to produce for instance a realistic Lagrangian velocity correlation and velocity-derivative skewness.

One typically finds for all time separations a value of the Lagrangian velocity correlation which is less than that of the Eulerian velocity correlation. As argued by Tennekes (1975), the temporal Eulerian autocorrelation that is recorded for small time separations is determined to a large extent by the process of sweeping of the

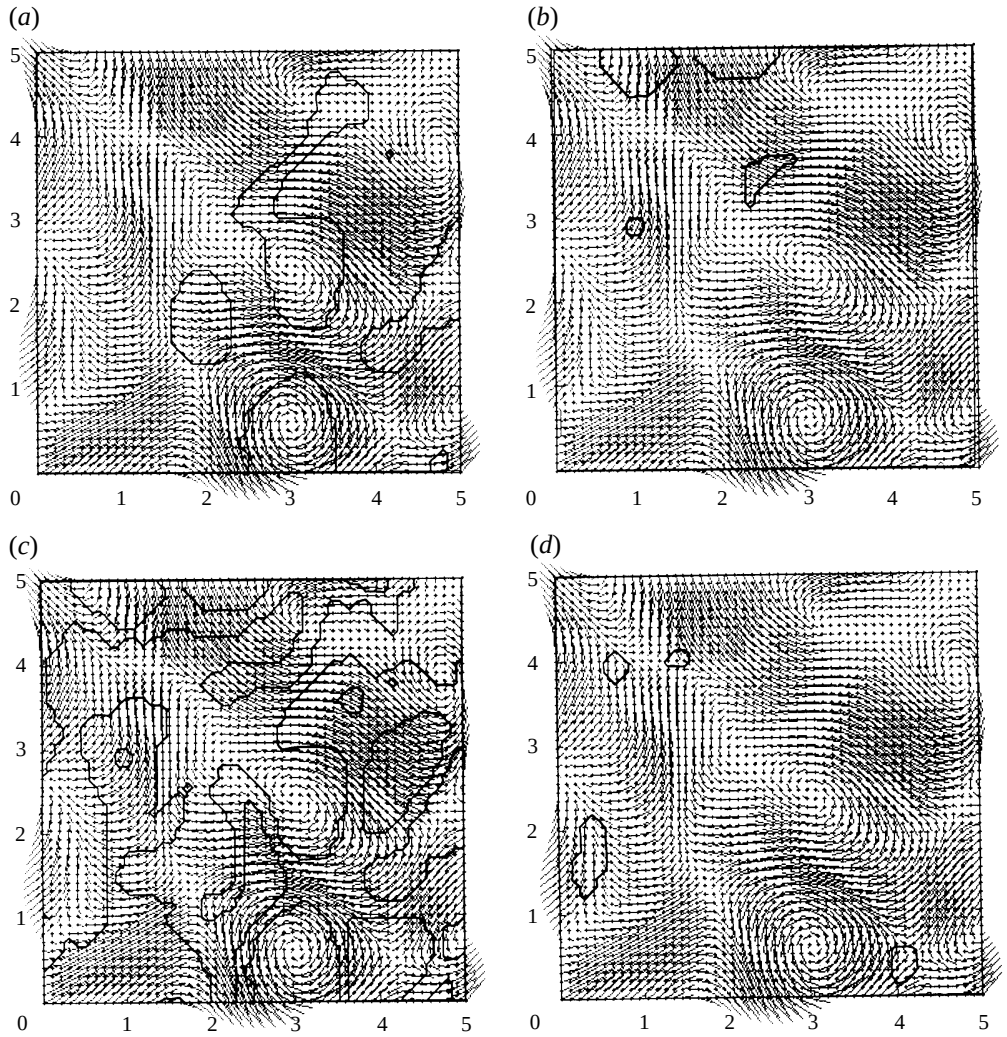

FIGURE 2. Two-dimensional snapshot of the three-dimensional velocity generated by a kinematic simulation using the Kraichnan spectrum function with $u_0 = 8.18$ cm s^{-1} and $L_{11} = 4.74$ cm. Coordinates are made dimensionless with L_{11}. (*a*) Eddy zones; (*b*) shear zones; (*c*) streaming zones; (*d*) convergence zones. The flow direction is along the small line elements, away from the dots that mark the base of these elements.

small scales past the observation point by the large-scale motions of the turbulence. On the other hand, over small time separations the velocity of a fluid particle remains reasonably well correlated. Thus it is expected that for small time separations the Eulerian velocity correlation function should lie below the Lagrangian autocorrelation function. A procedure to overcome this difficulty, by representing the dynamical process of sweeping of the small scales by the large scales within the method of kinematic simulation, has been devised by Fung *et al.* (1992). However, as it stands this rather time-consuming improvement leads for longer times to a decorrelation of the velocities at neighbouring points, and therefore cannot yet be used for our type of calculations. We believe that this is not really a drawback; in the problem studied

here the bubbles cut rapidly through fluid particle trajectories, so that the Eulerian structure is more important than the Lagrangian.

That a non-realistic velocity-derivative skewness, and thus a non-accurate representation of the instantaneous small-scale vorticity distribution, may seriously affect simulation results for small rigid particles has been demonstrated by Wang & Maxey (1993*a*). Whereas the kinematic simulations of Maxey (1987*a*) show an increase in the fall velocity of the particles over the fall velocity in quiescent fluid of at most 10%, the direct numerical simulations of Wang & Maxey (1993*a*) yield increased values up to 50% under comparable conditions. The difference is due to the fact that in the direct numerical simulations the turbulent flow evolves with the appropriate spatial and temporal structures, including the organized features of the dissipation-range dynamics. That these should be important was to be expected from Maxey's (1987*a*) approximate analyses, which show that the increased drift of the particles is related to higher-order velocity-derivative statistics.

For bubbles rising at high Reynolds numbers through turbulence with low intensity and characteristic length scales of the order of the length scale for the velocity relaxation of a bubble, it will be shown below that the dominant contribution to the statistics of the bubble motion is associated with the velocity autocorrelation function of the turbulence. This Eulerian property is represented well, of course, by our method of simulation, and a satisfactory agreement will be found between the analyses and the simulations when β, the ratio between the turbulence intensity and the rise velocity of the bubbles in still fluid, is small. For larger values of β it is conceivable that the instantaneous small-scale vorticity structure will become more important for the statistics of the bubble motion, especially in turbulence of high intensity ($\beta > 1$) when the bubble motion is governed by acceleration reaction forces. Our simulations concern the range $\beta \leqslant 1$, and although for these values of β the simulation results may require improvement quantitatively, we do believe that the overall behaviour of the statistics is represented well. This behaviour will be found to make sense, intuitively, and it is encouraging that for values of β close to 1 it shows the trends predicted by an approximate calculation for turbulence of high intensity and small characteristic length scales. We would like to emphasize that we welcome a check on our results by other methods of simulation.

3. Simulation of the motion of the bubbles

The equation governing the motion of small gas bubbles in liquids is still subject to discussion. When the characteristic Reynolds number of the bubble motion $Re = 2a|\boldsymbol{V} - \boldsymbol{U}|/\nu$ (a denoting the equivalent bubble radius) is high, and surface tension is large enough to keep the bubbles of spherical shape, it is sensible to use for practical purposes the equation of motion proposed by Thomas *et al.* (1984).

Bubbles with equivalent diameters of the order of 1 mm remain approximately spherical when rising steadily through water. The velocity of rise is about 25 cm s^{-1}, and the Reynolds number is $O(10^2)$. The drag coefficient in this case is $C_d = 48/Re + O(Re^{-3/2})$, and so the use of a linear drag law is a reasonable approximation, which defines the velocity of rise as $V_T = a^2 g/9\nu$, where g denotes the gravitational acceleration.

An approximate expression for the forces exerted on a rigid sphere in an unsteady inviscid rotational flow has been derived by Auton *et al.* (1988), under the assumptions that (i) changes in the fluid velocity on the scale of the sphere are small compared to the relative velocity, i.e. $a||\nabla \boldsymbol{U}|| \ll |\boldsymbol{V} - \boldsymbol{U}|$, and (ii) the length scale for changes

in the fluid velocity gradients is large compared with the sphere radius, i.e. $||\nabla \boldsymbol{U}|| \ll a||\nabla(\nabla \boldsymbol{U})||$. If the sphere has negligible mass its motion is described by the equation

$$\frac{\mathrm{d}\boldsymbol{V}}{\mathrm{d}t} = 3\frac{\mathrm{D}\boldsymbol{U}}{\mathrm{D}t} - (\boldsymbol{V} - \boldsymbol{U}) \times \boldsymbol{\Omega},$$

where $\mathrm{D}/\mathrm{D}t \equiv \partial/\partial t + \boldsymbol{U} \cdot \nabla$ is the fluid acceleration at the position of the bubble, and $\boldsymbol{\Omega} = \nabla \times \boldsymbol{U}$ is the vorticity.

The proposal of Thomas *et al.* (1984) is to combine this expression with the drag law mentioned above. One then obtains

$$\frac{\mathrm{d}\boldsymbol{V}}{\mathrm{d}t} = 3\frac{\mathrm{D}\boldsymbol{U}}{\mathrm{D}t} - (\boldsymbol{V} - \boldsymbol{U}) \times \boldsymbol{\Omega} - 2\boldsymbol{g} - \frac{1}{\tau_b}(\boldsymbol{V} - \boldsymbol{U}), \tag{3.1}$$

where the time constant τ_b is defined by $\tau_b = a^2/(18\nu) = V_T/(2g)$. For want of anything better we have adopted this equation for our simulations. It implies that the length scales of the turbulence should be large compared with the bubble radius. The ratio $1/a$ is indicated in figure 1. It is seen that the condition is met in most of the simulations; length scales of the velocity field that are smaller than the bubble radius may only occur in simulations that use the von Kármán–Pao spectrum with a fixed value of L_{11}.

3.1. *Dimensionless groups and simulation procedure*

The motion of gas bubbles through a turbulent flow may be characterized by the dimensionless groups (Hunt, Perkins & Fung 1994)

$$\frac{u_0}{V_T}, \quad \frac{L_{11}}{\tau_b V_T}, \quad \frac{T_L}{\tau_b},$$

which relate the relaxation time τ_b of the bubble to characteristic time scales of the turbulence. The integral length scale L_{11} is a measure of the size of the eddies in the flow, and thus of the spatial variation of the turbulence, whereas the integral time scale T_L is a measure of the time variation of the turbulence. When the rise velocity of a bubble is relatively small, a measure of this is the ratio $\beta = u_0/V_T$, the dimensionless group T_L/τ_b indicates whether the bubble responds quickly to the turbulent velocity fluctuations; it does so when the group has a large value. In what follows we have used that for grid turbulence $T_L/(L_{11}/u_0)$ is approximately constant, and have not considered T_L/τ_b as an independent group. We restrict ourselves to cases in which the turbulent intensity is less than the bubble rise velocity, i.e. $\beta \leqslant 1$. Especially when β is small, the rise velocity is large, and the bubble drifts easily through eddies; the relevant time scale for changes in the fluid velocity is then L_{11}/V_T. Thus it is the value of the dimensionless group $L_{11}/(\tau_b V_T)$ which is used here to indicate whether the bubble immediately adapts its speed to that of the fluid, rather than T_L/τ_b. It is also useful to introduce the group $\lambda/(\tau_b V_T)$ that can vary independently upon comparing different energy-spectrum functions. We therefore define

$$\beta = \frac{u_0}{V_T}, \quad \mu^* = \frac{L_{11}}{\tau_b V_T}, \quad \lambda^* = \frac{\lambda}{\tau_b V_T}.$$

Note that similar groups have been used by Nir & Pismen (1979) in an analysis of the dispersion of heavy particles.

In the simulations the velocity of the bubbles in quiescent fluid V_T is taken as 27.25 cm s^{-1} and the time constant τ_b as 13.9 ms; the equivalent radius a is then approximately equal to 0.5 mm. The consequences of changes in the structure of

the turbulence are studied by varying β, through variation of u_0, and by fixing the value of μ^*, that of λ^*, or both. In particular, in one set of simulations we took for the Kraichnan spectrum $\lambda^* = 4$ and $\mu^* = 2(2\pi)^{1/2} \simeq 5$, which means that the Taylor microscale is 15.1 mm and the longitudinal integral scale is 18.9 mm. The simulations with the von Kármán–Pao spectrum then either use the same value λ^*, i.e the same Taylor microscale, or the same value of μ^*, i.e. the same longitudinal integral scale. A second set of simulations used $\lambda^* = 1$ and $\mu^* = (\pi/2)^{1/2} \simeq \frac{5}{4}$ for the Kraichnan spectrum, and an equivalent procedure for the von Kármán–Pao spectrum.

The simulations were done with a 80486-processor based PC, equipped with a NDP VAST-2 Vectoriser and a Microway i860 Number Smasher. In each realization of the flow a single bubble is released with velocity V_T and its trajectory calculated with a fourth-order version of the Bulirsch–Stoer scheme (Press *et al.* 1991) over a sufficiently long time, typically of the order L_{11}/u_0, to allow the determination of the correlation functions. The best results for the statistical properties of the bubble motion were obtained by first time-averaging over each trajectory, where the origin was set at $t_0 \geqslant 5\tau_b$, and subsequently taking ensemble-averages over at least 200 realizations.

4. Mean velocity of the bubbles

The dimensionless deviation of the mean rise velocity $\overline{V}$ from its value in quiescent fluid is shown in figure 3. It appears that in the range of β considered here, the bubbles are on average slowed down by the turbulence, even to 50% of their velocity of rise in quiescent fluid. This effect is more prominent for the simulations with the Kraichnan spectrum than for those with the von Kármán–Pao spectrum with fixed Taylor microscale, and even more so for the simulations with the von Kármán–Pao spectrum with fixed longitudinal integral scale. For each of the spectra the mean bubble velocity diminishes with increasing turbulence intensity, i.e. down to a value of β roughly in the range 0.3 – 0.5. For higher values of the turbulence intensity the bubble velocity increases again or becomes approximately independent of β.

4.1. *Approximate analysis for large rise velocities*

To clarify the observed behaviour for small values of β one can use the theory in of Maxey (1987*a*, §4). From (3.1) it follows that the velocity difference $v_i = V_i - V_{Ti}$ is related to fluctuations in the fluid velocity u_i and vorticity ω_i by the equation

$$\frac{\mathrm{d}v_i}{\mathrm{d}t} = 3\left(\frac{\partial u_i}{\partial t} + u_j\frac{\partial u_i}{\partial x_j}\right) - \epsilon_{ijk}[V_{Tj} + (v_j - u_j)]\,\omega_k - \frac{1}{\tau_b}(v_i - u_i),$$

in which the subscripts can be x, y, z. Let $\mathscr{U}$, $\mathscr{L}$ be a typical velocity scale and length scale of the turbulence, and assume that we may take $\mathscr{L}/\mathscr{U}$ as a typical time scale of the turbulence. When $\mathscr{U}/V_T \ll 1$, a typical time scale of the fluid velocity fluctuations along the trajectories of the bubbles is $\mathscr{L}/V_T$, so that we have

$$(V_T/\mathscr{U})\frac{\mathrm{d}v_i'}{\mathrm{d}t'} = 3\left(\frac{\partial u_i'}{\partial t'} + u_j'\frac{\partial u_i'}{\partial x_j'}\right) - \epsilon_{ijk}[(V_T/\mathscr{U})e_j + (v_j' - u_j')]\,\omega_k' - (\mathscr{L}/\mathscr{U}\tau_b)(v_i' - u_i'). \quad (4.1)$$

Here the unit vector $\boldsymbol{e}$ points upwards, and the primes denote that the variables are dimensionless.

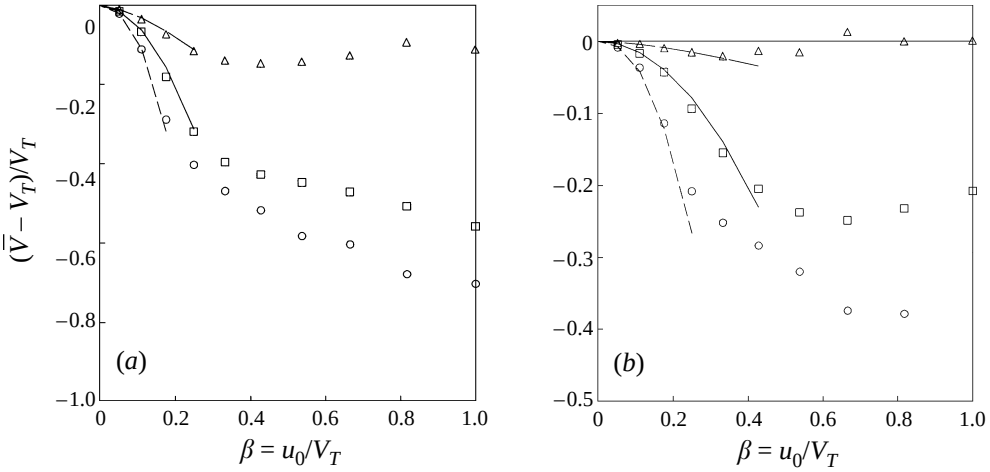

FIGURE 3. The difference between the mean velocity of rise of a bubble $\overline{V}$ in isotropic turbulence and its value in still fluid V_T, as a function of β. (*a*) □,——, Kraichnan spectrum with $\lambda^* = 1$ and $\mu^* = (\pi/2)^{1/2}$; △,— —, von Kármán–Pao spectrum with fixed Taylor microscale ($\lambda^* = 1$); ○,- - -, von Kármán–Pao spectrum with fixed integral scale ($\mu^* = (\pi/2)^{1/2}$). (*b*) As in (*a*) but with $\lambda^* = 4$ and $\mu^* = 2(2\pi)^{1/2}$. Curves show the analytical results for small β.

Now, assume that

$$\frac{\mathscr{U}}{V_T} \ll \frac{\mathscr{L}}{\tau_b V_T} \ll \frac{V_T}{\mathscr{U}},$$

which implies that the analysis is restricted to cases in which most of the turbulent energy is in intermediate length scales, as in the numerical simulations.

Following Maxey (1987*a*) one first expands the bubble path in terms of $\mathscr{U}/V_T$:

$$\boldsymbol{X}'(t') = \boldsymbol{X}'^{(0)}(t') + (\mathscr{U}/V_T)\boldsymbol{X}'^{(1)}(t') + (\mathscr{U}/V_T)^2\boldsymbol{X}'^{(2)}(t') + \cdots.$$

The lowest-order result, expressed in physical variables, is the straight path $\boldsymbol{X}^{(0)}(t) = \boldsymbol{V}_T t$. As pointed out by Maxey, the expansion is only valid as long as the deviation from the straight path $|\boldsymbol{X}(t) - \boldsymbol{X}^{(0)}(t)|$ is much smaller than a typical length scale in the turbulence. This is clearly the case if $\mathscr{U}/V_T$ is small enough: during the time that the bubble traverses a structure of size $\mathscr{L}$ (typically $\mathscr{L}/V_T$), $|\boldsymbol{X}(t) - \boldsymbol{X}^{(0)}(t)|$ is of $O(\mathscr{U}\mathscr{L}/V_T)$, which is small compared to $\mathscr{L}$.

Next, introduce an expansion for the fluid velocity along the bubble trajectory:

$$u_i'(\boldsymbol{X}'(t'), t') = u_i'(\boldsymbol{X}'^{(0)}(t'), t') + (\mathscr{U}/V_T)\boldsymbol{X}'^{(1)}(t') \cdot \nabla' u_i'(\boldsymbol{X}'^{(0)}(t'), t') + \cdots,$$

and a similar expansion for the vorticity, and substitute these in the dimensionless equation of motion of the bubbles. Under the above-mentioned assumptions this gives a set of equations for the coefficients of an expansion of the dimensionless bubble velocity,

$$\boldsymbol{v}'(t') = \boldsymbol{v}'^{(1)}(t') + (\mathscr{U}/V_T)\boldsymbol{v}'^{(2)}(t') + \cdots$$

of which the first two are

$$\frac{\mathrm{d}v_i'^{(1)}}{\mathrm{d}t'} = -\frac{\mathscr{L}}{\tau_b V_T}(v_i'^{(1)} - u_i'^{(0)}) - \epsilon_{ijk} e_j \omega_k'^{(0)}, \tag{4.2}$$

$$\frac{\mathrm{d}v_i'^{(2)}}{\mathrm{d}t'} = -\frac{\mathscr{L}}{\tau_b V_T}(v_i'^{(2)} - \boldsymbol{X}'^{(1)} \cdot \nabla' u_i'^{(0)}) - \epsilon_{ijk}(v_j'^{(1)} - u_j'^{(0)})\omega_k'^{(0)} + 3\left(\frac{\partial}{\partial t'} + u_j'^{(0)}\frac{\partial}{\partial x_j'}\right) u_i'^{(0)}. \tag{4.3}$$

Here $u_i'^{(0)} = u_i'(\boldsymbol{X}'^{(0)}(t'), t')$ and $\omega_i'^{(0)} = \omega_i'(\boldsymbol{X}'^{(0)}(t'), t')$.

The solution of equation (4.2) reads, in dimensional form,

$$v_i{}^{(1)}(t) = \int_0^t \mathrm{e}^{-(t-\tau)/\tau_b}\left\{\frac{1}{\tau_b}u_i{}^{(0)}(\tau) - V_T\epsilon_{ijk}e_j\omega_k^{(0)}(\tau)\right\}\mathrm{d}\tau, \tag{4.4}$$

from which

$$\frac{\mathscr{U}}{V_T}X_i{}^{(1)}(t) = \int_0^t \left\{1 - \mathrm{e}^{-(t-\tau)/\tau_b}\right\}\left\{u_i{}^{(0)}(\tau) - \tau_b V_T\epsilon_{ijk}e_j\omega_k^{(0)}(\tau)\right\}\mathrm{d}\tau, \tag{4.5}$$

which will be used below. As before, the unit vector $\boldsymbol{e}$ points upwards. The large-time-limit average of (4.2) yields

$$\overline{v_x^{(1)}} = \overline{u_x^{(0)}} = 0,$$

which shows that the deviation in the mean rise velocity is of order β^2.

Next by substituting (4.4) and (4.5) into equation (4.3) and taking the large-time limit one finds

$$\frac{\mathscr{U}}{V_T}\overline{v_x^{(2)}} = \frac{\mathscr{U}}{V_T}\overline{\boldsymbol{X}^{(1)} \cdot \nabla u_x^{(0)}} - \tau_b\epsilon_{xjk}\left(\overline{v_j^{(1)}\omega_k^{(0)}} - \overline{u_j^{(0)}\omega_k^{(0)}}\right)$$

$$= \tau_b V_T\int_0^\infty \frac{\partial^2 R_{xx}}{\partial x_j^2}(\tau \boldsymbol{V}_T; \tau)\mathrm{d}\tau$$

$$+\tau_b V_T\int_0^\infty \mathrm{e}^{-\tau/\tau_b}\left\{\frac{\partial R_{jj}}{\partial x_x} - \tau_b V_T\frac{\partial^2 R_{jj}}{\partial x_x^2}\right\}(\tau \boldsymbol{V}_T; \tau)\mathrm{d}\tau,$$

and

$$\frac{\mathscr{U}}{V_T}\overline{u_x^{(1)}} = \frac{\mathscr{U}}{V_T}\overline{\boldsymbol{X}^{(1)} \cdot \nabla u_x^{(0)}}$$

$$= \tau_b V_T\int_0^\infty \left\{1 - \mathrm{e}^{-\tau/\tau_b}\right\}\frac{\partial^2 R_{xx}}{\partial x_j^2}(\tau \boldsymbol{V}_T; \tau)\mathrm{d}\tau,$$

where $R_{ij}(\boldsymbol{x}; \tau) = \overline{u_i(\boldsymbol{0}; 0)u_j(\boldsymbol{x}; \tau)}$. With equations (3.4.5) and (3.4.6) of Batchelor (1953) these expressions can be rewritten to obtain

$$\overline{V} - V_T = 4\beta^2\tau_b V_T^2\int_0^\infty \frac{1}{r}\frac{\partial f}{\partial r}(r, r/V_T)\mathrm{d}r + O(\beta^3 V_T), \tag{4.6}$$

$$\overline{u_x} = \beta^2\tau_b V_T^2\int_0^\infty \left(1 - \mathrm{e}^{-r/\tau_b V_T}\right)\left\{\frac{\partial^2 f}{\partial r^2} + \frac{4}{r}\frac{\partial f}{\partial r}\right\}(r, r/V_T)\mathrm{d}r + O(\beta^3 V_T), \tag{4.7}$$

with $u_0^2 f(r, t) = R_{11}(r, 0, 0; t)$. If the time for a bubble to traverse L_{11} (typically L_{11}/V_T) is smaller than the time in which the fluid velocity starts to decorrelate (typically λ/u_0), the decorrelation in time of $f(r, \tau)$ may be neglected, i.e.

$$f(r, \tau) \approx f(r) \qquad \text{when } L_{11}\beta/\lambda \leqslant 1.$$

Using this approximation, and substituting equation (3.4.16) of Batchelor (1953)

finally yields

$$\overline{V} - V_T = \frac{1}{V_T}\int_0^\infty E(k)\chi(k\tau_b V_T)\mathrm{d}k + O(\beta^3 V_T L_{11}/\lambda), \tag{4.8}$$

$$\overline{u_x} = \frac{1}{V_T}\int_0^\infty E(k)\phi(k\tau_b V_T)\mathrm{d}k + O(\beta^3 V_T L_{11}/\lambda), \tag{4.9}$$

with the weighting functions

$$\chi(x) = -\tfrac{1}{2}\pi x,$$

$$\phi(x) = -1 - \tfrac{1}{2}\pi x + \left(-\frac{1}{x^3} - \frac{1}{x} + x\left(\frac{1}{x^2}+1\right)^2\right)\tan^{-1}x.$$

Note that in the case of the Kraichnan spectrum function (4.8) can be easily worked out further:

$$\overline{V} - V_T = -(8\pi)^{1/2}\beta^2 V_T\left(\frac{\tau_b V_T}{\lambda}\right) + O(\beta^3 V_T),$$

which explicitly shows the role of λ^*. The approximate expression (4.8) for the bubble velocity has been plotted in figure 3, and the agreement with the numerical results is satisfactory. The strongest decrease in the mean rise velocity occurs when using the von Kármán–Pao spectrum with a fixed value of L_{11}, and the smallest deviation occurs when the von Kármán–Pao spectrum is used with a fixed value of λ. The same order is found when comparing the values of $E(k)$ around $k = 1/(\tau_b V_T)$ in figure 1, which of course is due to the fact that in the simulations the energy density is highest at wavenumbers just below $1/(\tau_b V_T)$ and falls off strongly at higher wavenumbers.

The above analysis suggests the following mechanism for the reduction in the velocity of rise of the bubbles (see also figure 4): equation (4.2) describes how fluctuations in one component of the lateral vorticity cause bubbles to move under the action of lift forces in the other lateral direction, towards regions where the difference between the velocity of the bubble and that of the fluid is largest. In other words, since on average the bubbles move upwards they tend to move to regions where the downward fluid velocity has a maximum, and the upward velocity has a minimum. Equation (4.3) indicates that the lateral motion causes the bubbles to slow down on average because (i) viscous forces make the bubbles adapt their speed to the fluid velocity fluctuations, which on average are directed downwards along the bubble path, and (ii) this lateral motion induces a lift force in the downward direction. One would expect that as the Taylor microscale becomes smaller the mechanism will be more effective, since inertia forces such as the lift force become more important.

Results for the average vertical fluid velocity sampled by the bubbles are presented in figure 5. There is fair agreement with the analytical result (4.9). Note that the data for the different spectra 'cross' for $\beta > 0.2$, something which is not found in figure 3. Apparently the above-described mechanism ceases to be dominant as β becomes larger than 0.2; another, less effective, mechanism causes a reduction in the rise velocity. As one would expect and as suggested by figure 5, this mechanism is related to inertia forces other than the lift force.

4.2. *Trapping by vortices*

It is tempting to relate the decrease in the mean rise velocity of the bubbles, for $\beta > 0.2$, to the phenomenon of 'trapping by coherent vortices' observed by J. C. R. Hunt and his colleagues in mixing-layers (Thomas *et al.* 1984; Sene *et al.* 1994): every

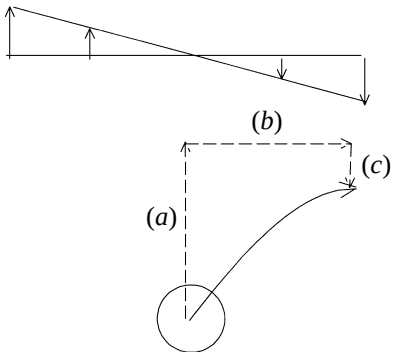

FIGURE 4. The mechanism by which weak turbulence causes fast rising bubbles to slow down on average. (*a*) As the bubble rises one component of the lateral vorticity induces a lift force in the opposite lateral direction. (*b*) This lift force pushes the bubble to where it meets the largest difference between the bubble rise velocity and the vertical fluid velocity. (*c*) The bubble slows down due to (i) the increased viscous drag force, and (ii) the lift force that is induced by the other component of the lateral vorticity as the bubble moves in the lateral direction.

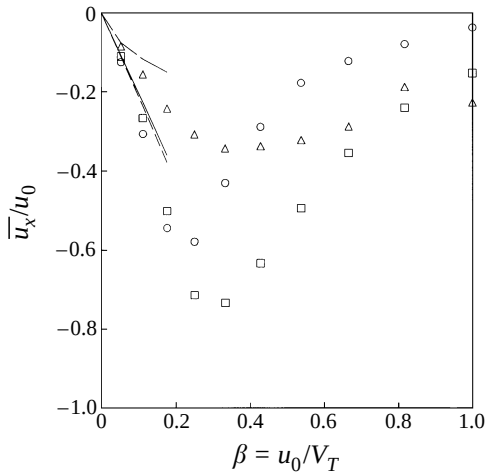

FIGURE 5. Average vertical fluid velocity along the bubble path, normalized by the turbulent intensity u_0, as a function of the ratio $\beta = u_0/V_T$. □,——, Kraichnan spectrum with $\lambda^* = 1$ and $\mu^* = (\pi/2)^{1/2}$; △,— —, von Kármán–Pao spectrum with fixed Taylor microscale ($\lambda^* = 1$); ○,- - - -, von Kármán–Pao spectrum with fixed integral scale ($\mu^* = (\pi/2)^{1/2}$). Curves show the analytical result for small β.

now and then a bubble slows down when it is trapped by a vortex, moves with it for a while, and then speeds up again as the vortex disintegrates. Similar observations have been made by Wang & Maxey (1993*b*) and Maxey, Chang & Wang (1994) for small bubbles in direct numerical simulations of isotropic turbulence (with $\beta \gg 1$).

To obtain evidence for this vortex trapping we have calculated the probabilities of finding the bubbles in the different zones mentioned in §2. These are presented in figure 6 for calculations with the Kraichnan spectrum function. The results are not conclusive. For small values of β the probabilities of finding a bubble in any of the zones merely equal the Eulerian values given in table 1. As β becomes larger (particularly for $\lambda^* = 4$) an increasing preferential concentration of bubbles in eddy zones indeed occurs, whereas the distribution of the various zones in the simulated

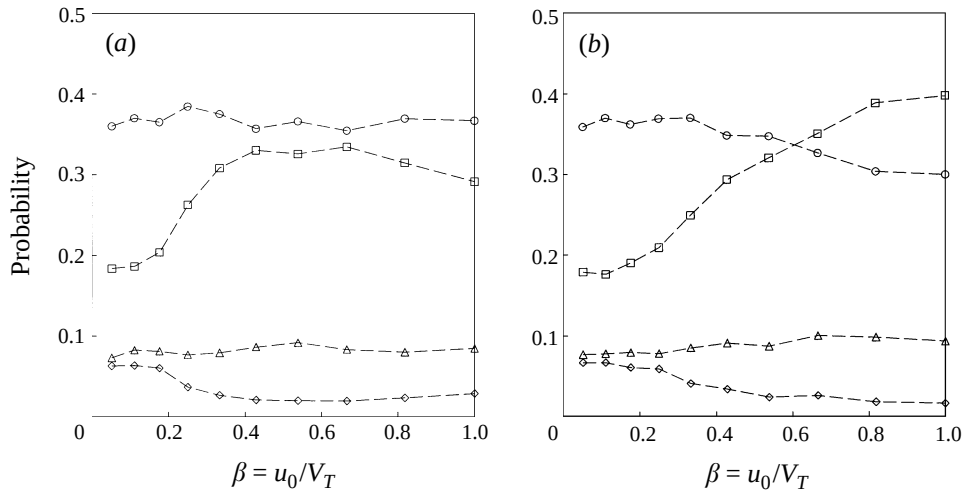

FIGURE 6. Probabilities of finding a bubble in zones of a turbulent flow following the classification of Wray & Hunt (1990). Simulations with the Kraichnan spectrum. (*a*) $\lambda^* = 1$; (*b*) $\lambda^* = 4$. □, Eddy zones; △, shear zones; ○, streaming zones; ◇, convergence zones.

turbulence remains the same. But this increase in the probability of being in eddy zones does not coincide with a decrease in mean bubble rise velocity as the value of β approaches 1.

Figure 7 shows two snapshots of the instantaneous fluid velocity field together with the positions of many non-interacting bubbles, in (*a*) for $\beta = 0.2$ and in (*b*) for $\beta = 0.8$, both from a calculation with a Kraichnan energy-spectrum function with $\lambda^* = 4$. The lower ends of the elongated structures formed by the bubbles in figure 7(*a*) coincide with downflow regions of the flow. In line with the mechanism advocated above, bubbles are transported to these downflow regions, where their velocity is significantly reduced; after escaping from these regions the bubbles follow approximately the same paths along which they accelerate back to a velocity close to V_T (cf. the discussion on figure 14). The elongated structures have disappeared in figure 7(*b*); here, an interesting feature is the higher concentrations of bubbles in the downwards flowing fluid on the edges of vortices. This suggests that for higher values of β the slowing down of the bubbles is indeed associated with the eddy zones; although the mechanism is presumably not that of trapping them in vortex cores, but rather transporting them towards the downwards flowing edges of the eddies, where the reduction of the velocity is predominantly caused by inertia forces and not by viscous forces. The phenomenon is reminiscent to what is found in Maxey (1987*b*) in cellular flows, albeit by using a different equation of motion for the bubbles. It will be clear that this interesting issue needs further investigation.

5. Dispersion of the bubbles

The longitudinal dispersion $D_x(t)$ of the bubbles about the mean displacement is defined by

$$D_x^2(t) = \overline{[X(t) - \overline{X}(t)]^2} = \overline{[X(t) - \overline{V}t]^2}.$$

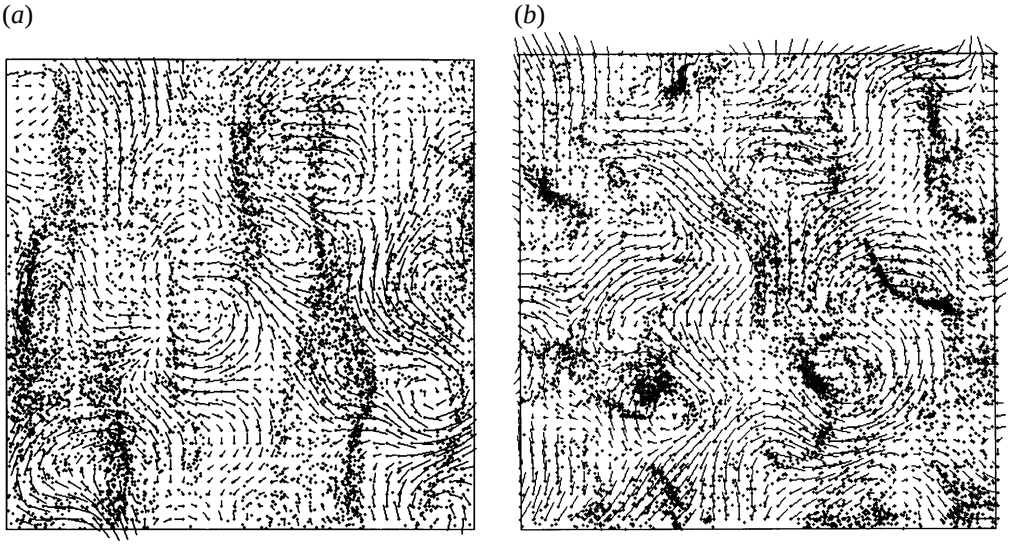

FIGURE 7. Bubble positions and instantaneous fluid velocity field in a plane through a cubic box of size 7.5 L_{11} containing 50,000 bubbles. Simulations done with the Kraichnan spectrum function with $\lambda^* = 4$ and (*a*) $\beta = 0.2$ and (*b*) $\beta = 0.8$. The flow direction is along the small line elements, away from the dots that mark the base of these elements.

For large values of t the dispersion process can be associated with a longitudinal diffusion coefficient defined as (Batchelor & Townsend 1956)

$$\mathscr{D}_x = \lim_{t\to\infty} \tfrac{1}{2}\frac{\mathrm{d}D_x^2}{\mathrm{d}t} = \int_0^\infty R_x(\xi)\,\mathrm{d}\xi.$$

$R(\xi)$ is the autocorrelation function of the fluctuation in the bubble velocity,

$$R_x(t-t') = \overline{[V_x(t)-\overline{V}][V_x(t')-\overline{V}]} = \overline{v_x(t-t')v_x(0)},$$

where in the last step we have used that the dispersion is a statistically stationary process; note that v as defined here differs from the v used in the previous section. By normalizing the autocorrelation function with the root-mean-square value of the bubble velocity fluctuation, the diffusion coefficient may be written as

$$\mathscr{D}_x = \overline{v_x^2}\mathscr{T}_x,$$

in which $\mathscr{T}_x$ is the longitudinal integral time scale for the bubble motion. Similar expressions hold for the lateral dispersion and diffusion coefficient.

5.1. *Approximate analysis for large rise velocities*

The analysis given in the previous section, for $\beta \ll 1$, also yields some approximate results for the dispersion of the bubbles. The deviation in the bubble velocity from its undisturbed value V_T, correct to $O(\beta u_0)$, is given by equation (4.4). Substituting this result into definitions given above and applying equation (3.4.5) of Batchelor (1953) yields for the longitudinal diffusion coefficient

$$\mathscr{D}_x = \beta u_0 L_{11} \;+\; O(\beta^2 u_0 L_{11}), \tag{5.1}$$

and for the lateral diffusion coefficient

$$\mathscr{D}_y = \tfrac{1}{2}\beta u_0 L_{11} \;-\; 2\tau_b^2 V_T u_0^2 \int_0^\infty \frac{1}{r}\frac{\partial f}{\partial r}\mathrm{d}r \;+\; O(\beta^2 u_0 L_{11}),$$

where $u_0^2 f(r) = R_{11}(r,0,0)$ and $r = V_T t$. Upon using equation (3.4.16) of Batchelor (1953) the latter expression can be rewritten as

$$\mathscr{D}_y = \tfrac{1}{2}\beta u_0 L_{11} \;+\; \tfrac{1}{4}\pi\tau_b^2 V_T \int_0^\infty kE(k)\mathrm{d}k \;+\; O(\beta^2 u_0 L_{11}). \tag{5.2}$$

These expressions coincide (as they should) with those derived by Csanady (1963) and Nir & Pismen (1979) for heavy solid particles, except for a contribution due to the lift force that induces a lateral motion, and which is seen to increase the lateral diffusivity. The lateral motion also leads, as explained in the previous section, to a reduction in the mean vertical velocity of the bubbles. Its effect on the longitudinal diffusivity is of higher order than taken into account in expression (5.2).

The intensities of the bubble velocity fluctuations are found to be equal to

$$\overline{v_x^2} = \int_0^\infty E(k)\phi_x(k\tau_b V_T)\mathrm{d}k \;+\; O(\beta u_0^2), \tag{5.3}$$

$$\overline{v_y^2} = \int_0^\infty E(k)\phi_y(k\tau_b V_T)\mathrm{d}k \;+\; O(\beta u_0^2) \tag{5.4}$$

with

$$\phi_x(x) = -\frac{1}{x^2} + \left(\frac{1}{x^3} + \frac{1}{x}\right)\tan^{-1}(x),$$

$$\phi_y(x) = \frac{1}{2} + \frac{1}{2x^2} - \left(\frac{1}{x} + \frac{1}{x^3} - \frac{x}{2}\left(\frac{1}{x^2}+1\right)^2\right)\tan^{-1}(x),$$

and the longitudinal and lateral integral time scales of the bubble velocity are given by

$$\mathscr{T}_x = \beta u_0 L_{11} \Big/ \int_0^\infty E(k)\phi_x(k\tau_b V_T)\mathrm{d}k\,, \tag{5.5}$$

$$\mathscr{T}_y = \left(\tfrac{1}{2}\beta u_0 L_{11} \;+\; \tfrac{1}{4}\pi\tau_b^2 V_T \int_0^\infty kE(k)\mathrm{d}k\right) \Big/ \int_0^\infty E(k)\phi_y(k\tau_b V_T)\mathrm{d}k\,. \tag{5.6}$$

It is seen from these expressions that $\overline{v_x^2}$ is mainly generated by the scales larger than the relaxation length $\tau_b V_T$, while $\overline{v_y^2}$ is mainly generated by scales smaller than $\tau_b V_T$.

A straightforward calculation next shows that for the Kraichnan spectrum function the longitudinal and lateral diffusion coefficients are given by, to first order in β,

$$\mathscr{D}_x \simeq \beta u_0 L_{11}, \qquad \mathscr{D}_y \simeq \tfrac{1}{2}\beta u_0 L_{11}[1 + 4(\tau_b V_T/\lambda)^2].$$

The intensities of the bubble velocity fluctuations are, if $\tau_b V_T/\lambda$ is small, approximately equal to

$$\overline{v_x^2} = u_0^2[1 - (\tau_b V_T/\lambda)^2], \qquad \overline{v_y^2} = u_0^2[1 + 3(\tau_b V_T/\lambda)^2],$$

from which it follows that the Lagrangian integral time scales are

$$\frac{\mathscr{T}_x}{(L_{11}/u_0)} \simeq \beta \frac{1}{1-(\tau_b V_T/\lambda)^2}, \quad \frac{\mathscr{T}_y}{(L_{11}/u_0)} \simeq \tfrac{1}{2}\beta \frac{1+4(\tau_b V_T/\lambda)^2}{1+3(\tau_b V_T/\lambda)^2}.$$

5.2. *Results of the simulations*

Numerical results for the diffusion coefficients are shown in figures 8 and 9, where as usual they have been normalized by $u_0 L_{11}$. Because of the 'crossing-trajectories effect' (Csanady 1963) the diffusion coefficients for small values of β are substantially

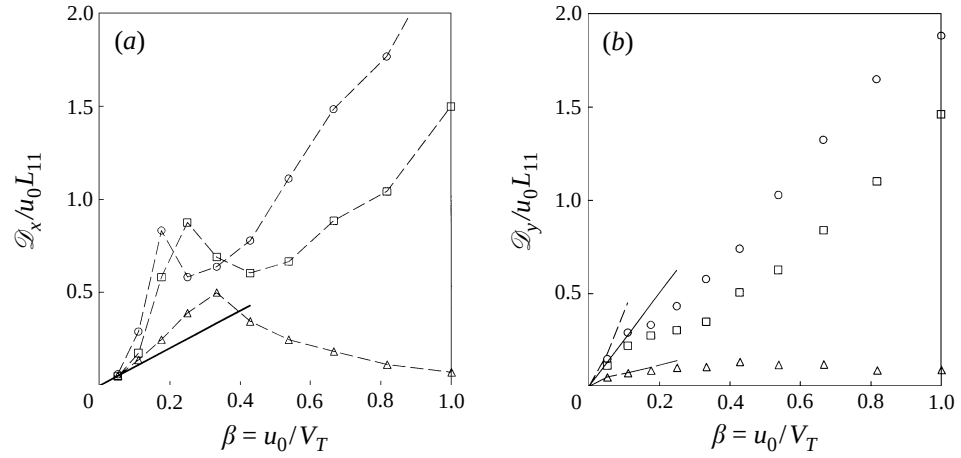

FIGURE 8. (*a*) Longitudinal and (*b*) lateral diffusion coefficients of the bubbles as a function of β. The diffusion coefficients are normalized with u_0 and the integral length scale L_{11}. □,——, Kraichnan spectrum with $\lambda^* = 1$ and $\mu^* = (\pi/2)^{1/2}$; △,— —, von Kármán–Pao spectrum with fixed Taylor microscale ($\lambda^* = 1$); ○,- - - -, von Kármán–Pao spectrum with fixed integral scale ($\mu^* = (\pi/2)^{1/2}$). Curves show to the analytical results.

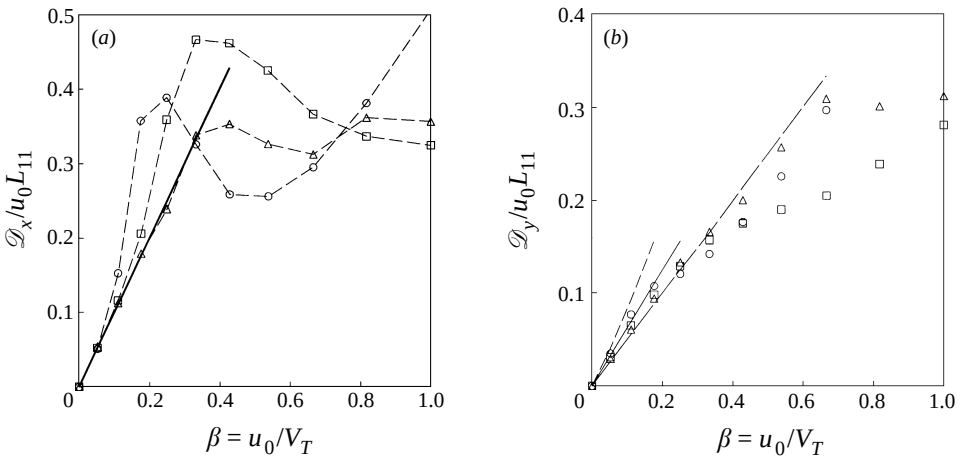

FIGURE 9. As figure 8 but with $\lambda^* = 4$ and $\mu^* = 2(2\pi)^{1/2}$.

lower than those of fluid particles, which are of the order u_0L_{11}. The diffusivities increase with increasing β, but level off when β becomes larger than about 0.25. However, for larger values of β, typically from between 0.4 and 0.8, the diffusivities are seen to increase without limit. Figures 10 and 11 give the intensities of the longitudinal and lateral bubble velocity fluctuations, normalized by the turbulence intensity u_0^2; figures 12 and 13 present the longitudinal and lateral integral time scales non-dimensionalized by L_{11}/V_T. We now briefly discuss some of the salient features of these figures; it should be said that more research is still needed to find a satisfactory explanation of all the details.

The first thing to notice is that the general appearance of the figures for the two different values of λ^* is the same, except that for the smaller value of the Taylor microscale changes in the trends occur at lower values of the non-dimensionalized

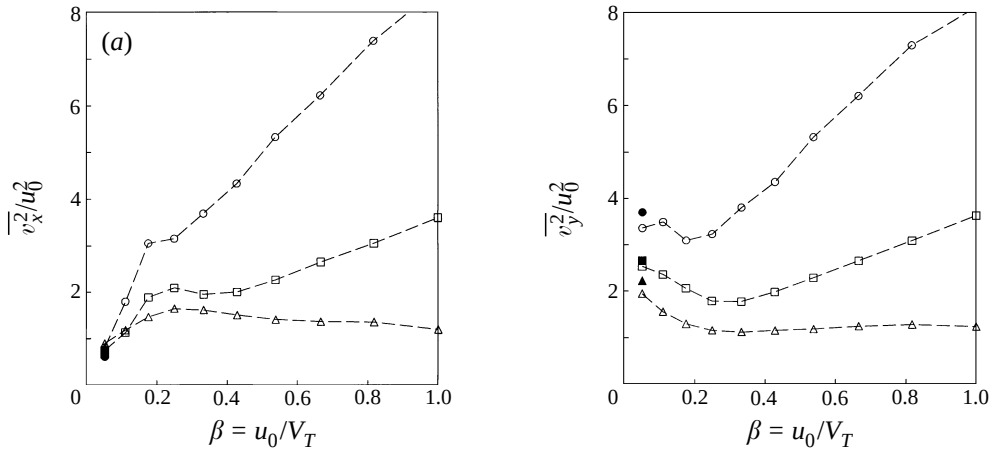

FIGURE 10. Ratios between the intensities of the (*a*) longitudinal and (*b*) lateral velocity fluctuations of the bubbles and the fluid, as a function of β. The data are presented as in figure 8 ($\lambda^* = 1$, $\mu^* = (\pi/2)^{1/2}$); filled symbols show the analytical result for small β.

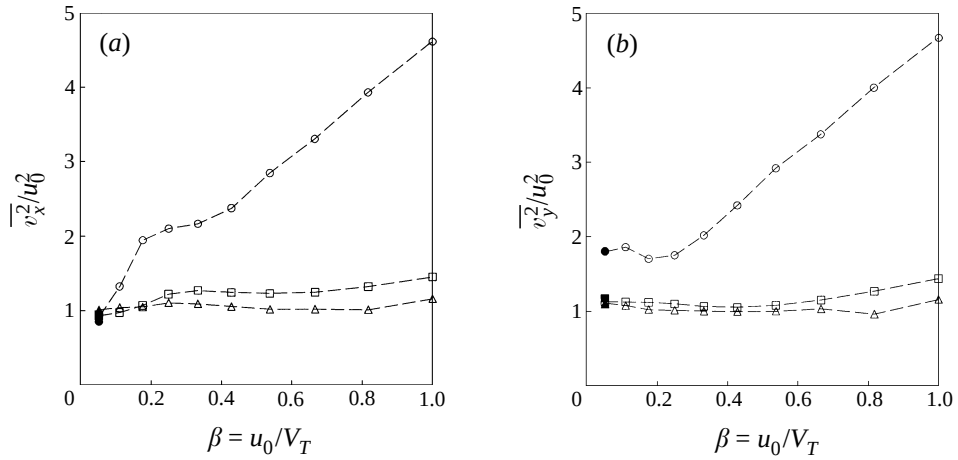

FIGURE 11. As figure 10 but for $\lambda^* = 4$, $\mu^* = 2(2\pi)^{1/2}$).

turbulence intensity β. This suggests that the gross features of the bubble statistics are related to the relative importance of the various inertia forces.

The results of the approximate analysis given above have been indicated in the figures; the agreement is satisfactory. At small values of β the longitudinal velocity fluctuations increase strongly with β. Upon comparing figures 10(*a*) and 11(*a*) with figure 3(*a*,*b*) it is seen that the relative magnitude of the increase in the velocity fluctuations between the different spectra is the same as that of the relative magnitude of the decrease in the mean rise velocities. In a way $\overline{v_x^2}$ is a measure of the range of values that the vertical velocities of the bubbles will have as they rise. The probability distribution of the vertical bubble velocity V_x is shown in figure 14 for two values of β, in both cases for a Kraichan spectrum with $\lambda^* = 1$. For comparison, the dashed lines show Gaussian distributions with corresponding mean and variance. The probability distribution function of V_x is close to Gaussian for $\beta = 0.53$, but for $\beta = 0.18$ we find an asymmetrical distribution with an enhanced preference for low values and values

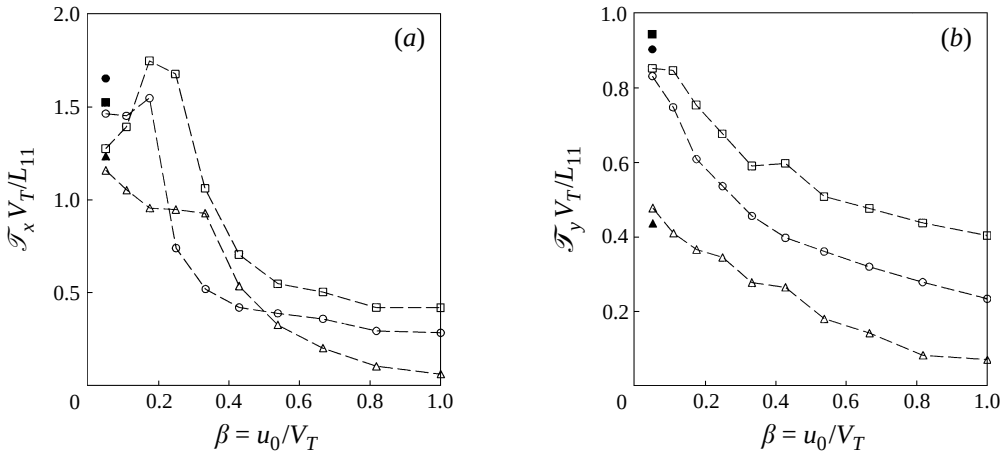

FIGURE 12. (*a*) Longitudinal and (*b*) lateral integral time scales of the bubble motion as a function of β. The data are presented as in figure 8 ($\lambda^* = 1$, $\mu^* = (\pi/2)^{1/2}$); filled symbols show to the analytical result for small β.

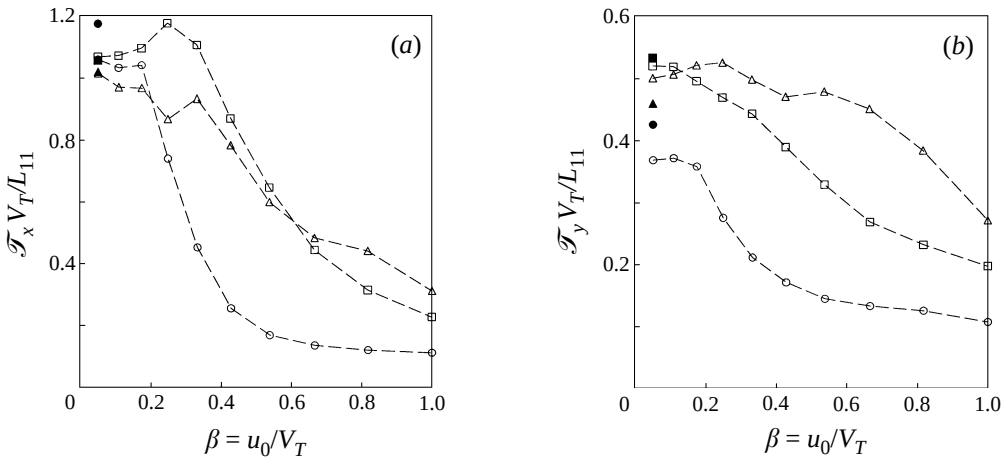

FIGURE 13. As figure 12 but for $\lambda^* = 4$, $\mu^* = 2(2\pi)^{1/2}$.

close to V_T. Thus the likely explanation of the increase of the longitudinal velocity fluctuations is that it is related to a slowing down of the bubbles in shear zones (by the mechanism explained in the previous section), and an accelerating back to a value close to V_T when the bubbles are outside these zones; these processes occur more often as the turbulence intensity increases.

The somewhat surprising fact that for small values of β the longitudinal integral time scales of the bubble motion first become larger as β increases, whereas those of the fluid become smaller, i.e. for the spectra with fixed longitudinal integral scale (see figures 12*a* and 13*a*), is probably associated with the reduction in the mean velocity of the bubbles. The lateral lift forces cause a bias in the velocity fluctuations sampled by the bubbles, which are therefore better correlated, and of course as the mean bubble velocity decreases the correlation of the fluid velocity along their trajectories improves.

For values of $\beta > 0.2$ the integral time scales for the bubble motion steadily

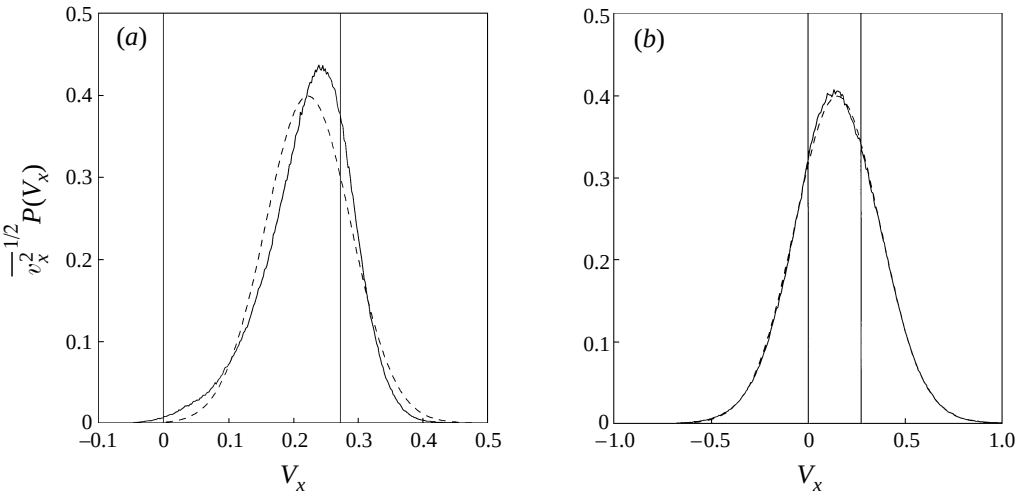

FIGURE 14. Probability distribution of the vertical bubble velocity V_x in simulations using the Kraichnan spectrum with $\lambda^* = 1$ and (*a*) $\beta = 0.18$ and (*b*) $\beta = 0.53$. Dashed lines are Gaussian probability distribution functions with corresponding mean and variance. Vertical lines indicate $V_x = 0$ and $V_x = V_T$, the velocity of rise in still fluid.

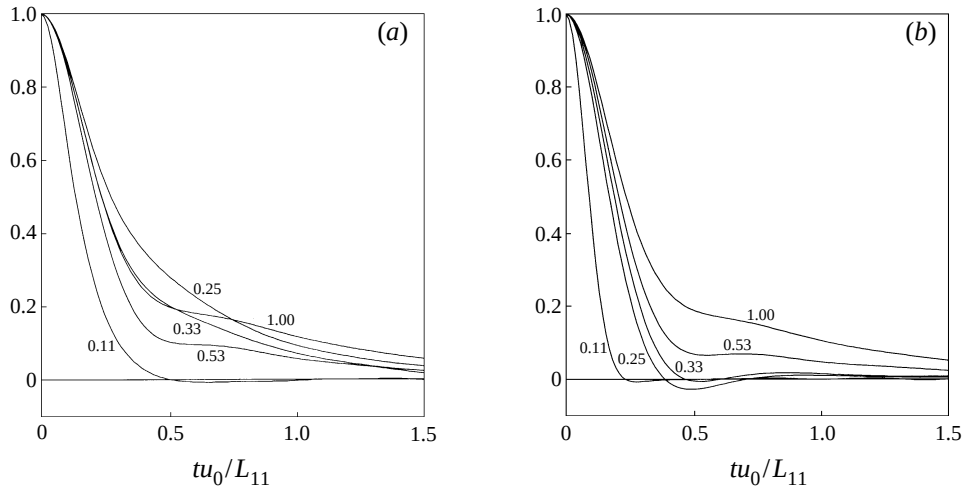

FIGURE 15. (*a*) Longitudinal and (*b*) lateral bubble velocity correlations when using the Kraichnan spectrum (with $\lambda^* = 1$). Numbers refer to values of β.

decrease, and they do this faster than the integral time scales for the motion of fluid particles. Figure 15, the longitudinal and lateral bubble velocity correlations, shows that this rapid decrease is caused by a reduction of the correlation of the bubble velocity over large times; the fluid velocity fluctuations along the bubble trajectories appear to remain well correlated over these larger times as can be seen in figure 16. This is another indication of the significant role of the acceleration reaction forces for larger values of β, which prevent the bubbles adapting their velocity to that of the surrounding fluid. The reduction of the bubble diffusivities for values of β in the range 0.2–0.4 is presumably related to the observed decrease in the Lagrangian integral time scales.

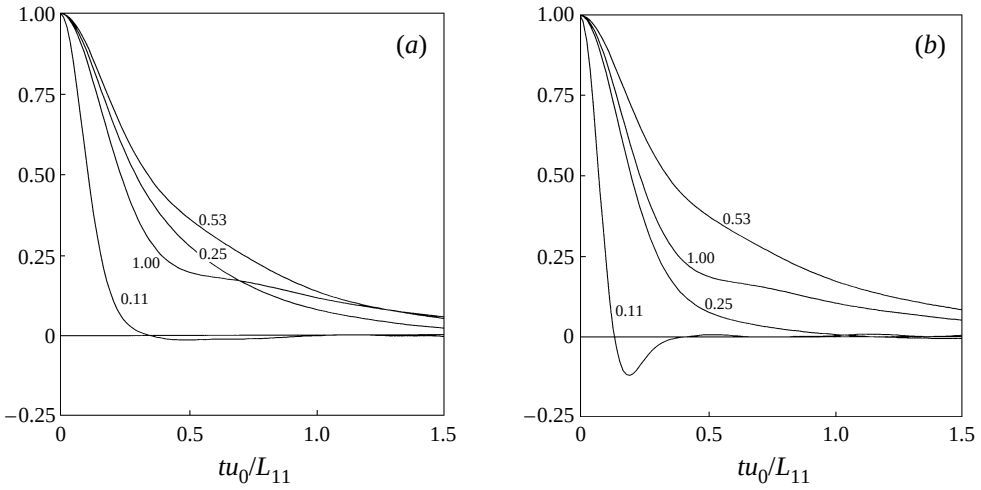

FIGURE 16. (*a*) Longitudinal and (*b*) lateral fluid velocity correlations along the bubble path when using the Kraichnan spectrum ($\lambda^* = 1$). Numbers refer to values of β.

The most remarkable feature of the results for $\beta > 0.4$ is a 'blow-up' of the bubble velocity fluctuations as β increases, and as a result of this the bubble diffusivities are again strongly raised. The effect can be seen most clearly in the simulations with the von Kármán–Pao spectrum function with fixed longitudinal integral scale: $\overline{v^2}$ increases even with respect to u_0^2. This interesting behaviour is further addressed below.

5.3. *Blow-up of the velocity fluctuations*

We seek to explain why for sufficiently large values of β the velocity fluctuations of the bubble become isotropic, and increase enormously in magnitude, by using a simple model equation:

$$\frac{\mathrm{d}v_i}{\mathrm{d}t} = -\frac{1}{\tau_b}(v_i - u_i) + L_i(t), \tag{5.7}$$

in which the random force $L_i(t)$ does not explicitly depend on τ_b, and decorrelates in a time that is much smaller than τ_b. This because as β increases the relaxation time of the bubbles becomes large compared with the characteristic time scales of the turbulence. The main simplification is that $L_i(t)$ does not depend on $v_i(t)$, for instance as it appears in the expression for the lift force; we believe that that contribution plays no role in the blow-up of the bubble velocity fluctuations. Another simplification is that the model equation is one-dimensional, a choice motivated by the observed isotropy of the fluctuations.

Dropping the indices, we have

$$\begin{aligned}\overline{v^2}(t) \approx{}& \frac{1}{\tau_b^2}\int_0^t\int_0^t \mathrm{e}^{-|t-t'|/\tau_b-|t-t''|/\tau_b}\overline{u(0)u(t''-t')}\mathrm{d}t'\mathrm{d}t''\\ &+\frac{1}{\tau_b}\int_0^t\int_0^t \mathrm{e}^{-|t-t'|/\tau_b-|t-t''|/\tau_b}\left(\overline{u(0)L(t''-t')}+\overline{L(0)u(t''-t')}\right)\mathrm{d}t'\mathrm{d}t''\\ &+\int_0^t\int_0^t \mathrm{e}^{-|t-t'|/\tau_b-|t-t''|/\tau_b}\overline{L(0)L(t''-t')}\mathrm{d}t'\mathrm{d}t''.\end{aligned}$$

Changing the order of integration, and then using that τ_b is much larger than a

typical time over which the integrand is correlated, which implies that $\mathrm{e}^{-|t''-t'|/\tau_b}$ can be replaced by 1 and the limit $t \to \infty$ can be taken, yields

$$\overline{v^2} \approx \int_0^\infty \left(\frac{1}{\tau_b} \overline{u(0)u(s)} + \overline{u(0)L(s)} + \overline{L(0)u(s)} + \tau_b \overline{L(0)L(s)} \right) \mathrm{d}s.$$

Clearly, the last term is dominant and leads to a blow-up of $\overline{v^2}$. A comparison of the model equation (5.7) with the equation of motion of a bubble (3.1) shows that $L(t)$ is of order $u_0^2/\mathscr{L}$, with $\mathscr{L}$ some characteristic length scale of the turbulence, and that the integral time scale of $L(t)$ is of order $\mathscr{L}/u_0$, so that

$$\overline{v^2} \approx \tau_b \int_0^\infty \overline{L(0)L(s)}\, \mathrm{d}s \;=\; O\left(\frac{\tau_b u_0^3}{\mathscr{L}} \right) \;=\; O\left(\beta u_0^2 \frac{\tau_b V_T}{\mathscr{L}} \right).$$

Since in the simulations either λ^* or μ^* (or both) are kept constant, $\tau_b V_T/\mathscr{L}$ is approximately constant and the result agrees well with the linear dependence on β of the dimensionless velocity fluctuations found for sufficiently large β.

The physical explanation of the observed behaviour is that very rapidly changing (inertial) driving forces tend to 'spread out' the velocities of the bubbles, an effect which is resisted by the viscous drag forces. But as the relative magnitude of the relaxation time of the bubbles becomes larger the first effect will become dominant, and the bubble velocity fluctuations will grow. The phenomenon also occurs when a heavy molecule is immersed in a fluid of light molecules (see van Kampen 1992, pp. 219–221).

By a similar analysis it is also possible to calculate the velocity correlation for the model system. The result is

$$\lim_{t\to\infty} \overline{v(t)v(t+\tau)} \;\approx\; \overline{v^2} \mathrm{e}^{-\tau/\tau_b},$$

for time separations τ much larger than the integral time scale of $L(t)$. If it is assumed that this provides a reasonable estimate for all values of τ, the bubble diffusivities and integral time scales are found to be

$$\mathscr{D} = O\left(u_0 \mathscr{L} \beta^2 \, (\tau_b V_T/\mathscr{L})^2 \right), \qquad \mathscr{T} = O(\tau_b),$$

which is indeed observed in the simulations when the characteristic length scales of the turbulence are small.

Whether the predicted blow-up can be observed in experiments is doubtful; the applicability of the equation of motion of the bubbles is of course questionable for turbulence of high intensity at small length scales.

The authors would like to thank Alex Joia and Richard Perkins (Ecole Centrale de Lyon) for valuable discussions on the method of kinematic simulation, made possible by financial support of the EC under the programme Human Capital and Mobility. We are also grateful to Leen van Wijngaarden for enlightening discussions and Wim Gorissen for drawing our attention to the Bulirsch–Stoer scheme.

This work is part of the research program of the "Stichting voor Fundamenteel Onderzoek der Materie (FOM)", which is financially supported by the "Nederlandse organisatie voor wetenschappelijk onderzoek (NWO)".

REFERENCES

Auton, T. R., Hunt, J. C. R. & Prud'homme, M. 1988 The force exerted on a body in inviscid unsteady non-uniform rotational flow. *J. Fluid Mech.* **197**, 241–257.

Batchelor, G. K. 1953 *The Theory of Homogeneous Turbulence*. Cambridge University Press.

Batchelor, G. K. & Townsend, A. A. 1948 Decay of turbulence in the final period. *Proc. R. Soc. Lond.* A **194**, 527–543.

Batchelor, G. K. & Townsend, A. A. 1956 Turbulent diffusion. In *Surveys in Mechanics* (ed. G. K. Batchelor & R. M. Davies), pp. 352–399. Cambridge University Press.

Csanady, G. T. 1963 Turbulent diffusion of heavy particles in the atmosphere. *J. Atmos. Sci.* **20**, 201–208.

Fung, J. C. H. 1993 Gravitational settling of particles and bubbles in homogeneous turbulence. *J. Geophys. Res.* **98**, 20287–20297.

Fung, J. C. H., Hunt, J. C. R., Malik, N. A. & Perkins, R. J. 1992 Kinematic simulation of homogeneous turbulence by unsteady random Fourier modes. *J. Fluid Mech.* **230**, 281–318.

Helland, K. N., Van Atta, C. W. & Stegen, G. R. 1977 Spectral energy transfer in high Reynolds number turbulence. *J. Fluid Mech.* **79**, 337–359.

Hunt, J. C. R., Buell, J. C. & Wray, A. A. 1987 Big whorls carry little whorls. *NASA Rep.* CTR-S87.

Hunt, J. C. R., Perkins, R. J. & Fung, J. C. H. 1994 Problems in modeling disperse two-phase flows. *Appl. Mech. Rev.* **47**, S49-S60.

Hunt, J. C. R., Wray, A.A. & Moin, P. 1988 Eddies, streams, and convergence zones in turbulent flows. *NASA Rep.* CTR-S88.

van Kampen, N. G. 1992 *Stochastic Processes in Physics and Chemistry*, 2nd edn., North-Holland.

Kraichnan, R. H. 1970 Diffusion by a random velocity field. *Phys. Fluids* **13**, 22–31.

Maxey, M. R. 1987*a* The gravitational settling of aerosol particles in homogeneous turbulence and random fields. *J. Fluid Mech.* **174**, 441–465.

Maxey, M. R. 1987*b* The motion of small spherical particles in a cellular flow field. *Phys. Fluids* **30**, 1915–1928.

Maxey, M. R., Chang, E. J. & Wang, L.-P. 1994 Simulation of interactions between microbubbles and turbulent flows. *Appl. Mech. Rev.* **47**, S70-S74.

Mei, R. 1994 Effect of turbulence on the particle settling velocity in the nonlinear drag range. *Intl J. Multiphase Flow* **20**, 273-284.

Moore, D. W. 1963 The boundary layer on a spherical gas bubble. *J. Fluid Mech.* **23**, 161–176.

Nir, A. & Pismen, L. M. 1979 The effect of a steady drift on the dispersion of a particle in turbulent fluid. *J. Fluid Mech.* **94**, 369–381.

Press, W. H., Flannery, B. P., Teukolski, S. A. & Vetterling, W. T. 1991 *Numerical Recipes in PASCAL*. Cambridge University Press.

Sene, K. J., Hunt, J. C. R. & Thomas, N. H. 1994 The role of coherent structures in bubble transport by turbulent shear flows. *J. Fluid Mech.* **259**, 219–240.

Spelt, P. D. M. 1996 The motion of bubbles in a turbulent flow. PhD Thesis, University of Twente.

Sreenivasan, K. R. 1984 On the scaling of the turbulence energy dissipation rate. *Phys. Fluids* **27**, 1048–1051.

Tennekes, H. 1975 Eulerian and Lagrangian time microscales in isotropic turbulence. *J. Fluid Mech.* **67**, 561–567.

Thomas, N. H., Auton, T. R., Sene, K. J. & Hunt, J. C. R. 1984 Entrapment and transport of bubbles in plunging water. In *Gas Transfer at Water Surfaces* (ed. W. Brutsaert & G. H. Jurka), pp. 255–268. D. Reidel.

Wang, L.-P. & Maxey, M. R. 1993*a* Settling velocity and concentration distribution of heavy particles in homogeneous isotropic turbulence. *J. Fluid Mech.* **256**, 27-68.

Wang, L.-P. & Maxey, M. R. 1993*b* The motion of microbubbles in a forced isotropic and homogeneous turbulence. *Appl. Sci. Res.* **51**, 291-296.

Wang, L.-P. & Stock, D. E. 1994 Numerical simulation of heavy particle dispersion – Scale ratio and flow decay considerations. *Trans. ASME: J. Fluids Engng* **116**, 154–163.

Wray, A.A. & Hunt, J. C. R. 1990 Algorithms for classification of turbulent structures. In *Topological Fluid Mechanics* (ed. H. K. Moffatt & A. Tsinober), pp. 95–104. Cambridge University Press.